Design and Prototyping of a Low-Cost Spacecraft Attitude Determination and Control Setup

A project present to
The Faculty of the Department of Aerospace Engineering
San Jose State University

in partial fulfillment of the requirements for the degree
Master of Science in Aerospace Engineering

By

Anthony Gong

May 2015

approved by

Dr. Kamran Turkoglu
Faculty Advisor

The Designated Project Committee Approves the Project Titled

DESIGN AND PROTOTYPING OF A LOW-COST SPACECRAFT ATTITUDE DETERMINATION AND CONTROL SETUP

By

Anthony Gong

APPROVED FOR THE DEPARTMENT OF AEROSPACE ENGINEERING

SAN JOSE STATE UNIVERSITY

MAY 2015

_____   _____

Dr. Kamran Turkoglu, Project Advisor   Date
Department of Aerospace Engineering

Preliminary Design and Prototyping of a Low-Cost Spacecraft Attitude Determination and Control Setup

Anthony Gong   and Kamran Turkoglu [y]
San Jose State University, San Jose, CA 95192, USA

In current literature, various ground-based spacecraft attitude determination and con-trol setups are employed to test control strategies and algorithms. However, they typically require relatively large amounts of clearance for rotation and are prohibitively expensive for academic/research use. In this paper, we outline the development of a 1-D prototype that aims to serve as a low-cost alternative. The goal is to develop an open-source, low-cost platform at minimal cost. The prototype consists of an aluminum wheel driven by a brush-less DC motor mounted to a plate that is allowed to pivot about a hinge. The prototype has the ability to transfer angular momentum between the wheel and the body as well as balance using reaction torques. PID and LQR controllers for the prototype have been designed to achieve minimal control e ort. Preliminary results demonstrate that the LQR is able to achieve energy savings of 8% over the baseline PID controller with acceptable tradeo s. Experimental results show that a LQR augmented with integral action is able to reject disturbances and successfully balance. The 1-D prototype remains low-cost at $480.

Nomenclature

C   dynamic friction coe cient
g gravitational acceleration h
angular momentum
Imoment of inertia

l   distance from pivot point
m mass
T   torque
u   input current
angle or position
$\dot{}$ angular velocity
angular acceleration
( )$_b$ body-related parameter
( )$_w$ wheel/rotor assembly-related parameter

I.   Introduction

All spacecraft require some form of stabilization and control due to the external disturbances in space. Stabilization can be achieved through various methods such as gravity-gradient,[1] spin,[2] and 3-axis stabi-lization,[3] where control of the spacecraft is achieved through passive[4] or active[5] actuators such as magnetic torque rods, reaction thrusters, and reaction wheels.

Before deployment in space, spacecraft must be tested extensively through ground-based equipment that attempt to simulate the environment. These setups typically involve a rotating air-bearing table designed

---

Graduate student, Aerospace Engineering, anthony.gong@sjsu.edu.
[y] Assistant Professor, Department of Aerospace Engineering, kamran.turkoglu@sjsu.edu

American Institute of Aeronautics and Astronautics

to mitigate the e ects of gravity.[6{9] However, these setups usually require relatively large amounts of space for rotation and are excessively expensive (where $20,000 is considered low-cost).[10]

There are novel spacecraft attitude control setups currently found in literature. 3D reaction wheel con gurations[11] and three axis control via two reaction wheels are some of the recent research e orts.[12{14] Various con gurations with four reaction wheels have also been investigated for lowest energy consumption.[15] Inverted pendulums have been developed to study control algorithms and strategies. Amongst these designs, there are some that utilize reaction wheels and their associated reaction torques to self-erect and balance.[16{18] It is possible to utilize existing setups in literature to design one from scratch, which can serve as an experimental, low-cost research and education platform for spacecraft attitude determination and control studies. Previously developed Cubli[17] is a prime example and the primary motivation for the current design.

The design would need to satisfy several requirements. It must be as unobstructive as possible (can t on a small desk). It must be a ordable such that academic institutions and even students can purchase the components and construct the suggested set-up on their own. The setup should also draw minimal power to be representative of a spacecraft with a limited power budget.

The nal product of our work is a 6-inch cube that contains the attitude determination and control system of a typical 3-axis stabilized spacecraft. Three 1-D (one degree of freedom) prototypes are mounted orthogonally to provide 3-axis control. The 1-D prototype is manufactured rst to evaluate the mathematical model and assess its performance before proceeding to a full 3-D assembly.

The main aim of this paper is to present a low-cost spacecraft attitude determination and control setup which could be utilized in research and education. For analytical purposes, the corresponding equations of motion and an overview of the design is described in Section II. In Section III, various controller designs are investigated and with the preliminary results given in Section V, the paper is concluded.

II.   1-D Prototype Analysis and Design

One essential constraint of our work is that the designed setup must operate in such a fashion that it mimics the conditions in space where gravity is negligible. In the vertical equilibrium position, gravity will not apply any torques as the center of mass of the setup is directly over the pivot point. As long as the tilt angle remains small, gravitational e ects will be minor, and the setup can be assumed to be operating in a space-like environment.

The prototype consists of a reaction wheel driven by a brushless DC motor that is mounted to the center of a square metal plate (spacecraft body). The self-erecting setup utilizes reaction torques for balancing and a braking mechanism to impulsively transfer angular momentum for the initial jump-up maneuver.

A. Equations of Motion

Knowing that angular momentum and torque can be expressed as,[19]

$$h = I\bar{\omega} \tag{1}$$

$$T = I\dot{\omega} \tag{2}$$

the equations of motion, as previously presented,[17] can be derived from the free-body diagram shown in Fig. 1 as

$$\dot{\theta}_b = \frac{-(m_b l_b + m_w l_w)\, g \sin\theta_b\ T_m\ C_b\, \bar{\theta}_b + C_w\, \bar{\theta}_w}{I_b + m_w l_w^2} \tag{3}$$

$$\dot{\theta}_w = \frac{(I_b + I_w + m_w l_w^2)(T_m\ C_w\, \bar{\theta}_w)}{I_w(I_b + m_w l_w^2)}\ \frac{(m_b l_b + m_w l_w)\, g \sin\theta_b\ C_b\, \bar{\theta}_b}{I_b + m_w l_w^2} \tag{4}$$

where m_w is the mass of the wheel and m_b is the mass of all other components minus the hinge assembly. l_w and l_b are the distances from the pivot point to the center of mass of the wheel and pendulum body, respectively. θ_b is the tilt angle measured from the local vertical and θ_w is the arbitrary position of the wheel relative to some point on the body. Unlike its time derivative, $\bar{\theta}_w$, which is the angular velocity of the reaction wheel, θ_w is a variable that will be derived but not used as a state. Here, T_m is the torque of the motor and it is de ned in Eq. (5)
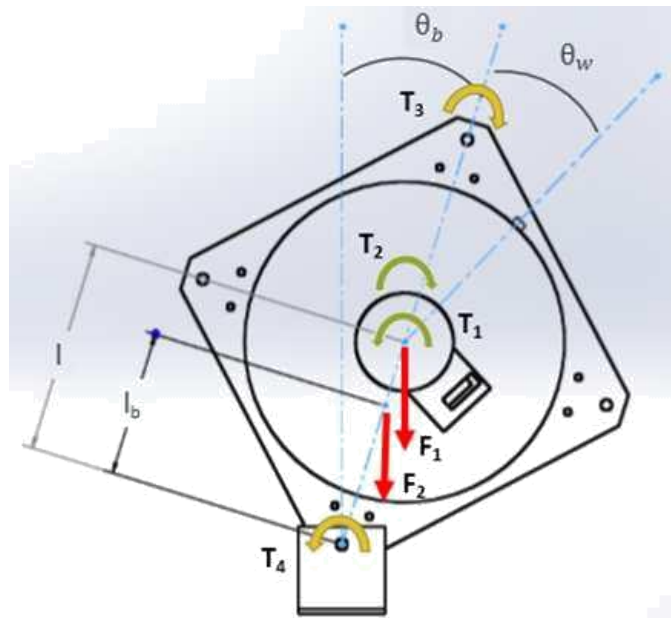
$$T_m = K_m u \tag{5}$$

American Institute of Aeronautics and Astronautics

Figure 1. Free-body diagram of the 1-D prototype.

From the general form of a dynamic system,[19]

$$\dot{x} = Ax + Bu$$
$$y = Cx + Du$$

(6)

Eqs. (3) and (4) are linearized about the vertical equilibrium point,

$$(\theta_b; \dot{\theta}_b; \dot{\theta}_w) = (0; 0; 0)$$

(7)

and the state space representation is given in Eq. (8).[17]

$$
\begin{bmatrix} \dot{\theta}_b \\ \ddot{\theta}_b \\ \ddot{\theta}_w \end{bmatrix} =
\begin{bmatrix}
0 & 1 & 0 \\
\frac{(m_b l_b + m_w l_w)g}{I_b + m_w l_w^2} & \frac{C_b}{I_b + m_w l_w^2} & -\frac{C_w}{I_b + m_w l_w^2} \\
-\frac{(m_b l_b + m_w l_w)g}{I_b + m_w l_w^2} & \frac{C_b}{I_b + m_w l_w^2} & \frac{C_w(I_b + I_w + m_w l_w^2)}{I_w(I_b + m_w l_w^2)}
\end{bmatrix}
\begin{bmatrix} \theta_b \\ \dot{\theta}_b \\ \dot{\theta}_w \end{bmatrix}
+
\begin{bmatrix}
0 \\
-\frac{K_m}{I_b + m_w l_w^2} \\
\frac{K_m(I_b + I_w + m_w l_w^2)}{I_w(I_b + m_w l_w^2)}
\end{bmatrix} u
$$

(8)

Table 1 summarizes the system parameters that have been identified. The lengths and masses are easily determined through simple experiments. The moments of inertia are estimated by Solidworks[20] after applying material properties to each component. I_w is found by summing the moments of inertia of the aluminum disk and DF45. The friction coefficients are found through experimentation and Eqs. (9)-(10).[17]

$$I_w \dot{\omega}_w(t) = K_m u(t) - C_w \dot{\omega}_w(t)$$

(9)

$$(I_b + I_w + m_w l_w^2)\ddot{\theta}_b(t) = -C_b \dot{\theta}_b(t) + (m_b l_b + m_w l_w)g \sin \theta_b(t)$$

(10)

B. Prototype Design

As shown in Fig. 3, the setup is capable of impulsively transferring angular momentum from the wheel assembly to the body through the use of a braking mechanism. Such a transfer will cause the setup to pop up from its initial resting position and travel 45 to the vertical position, which is depicted in Fig. 2.

To accomplish this, careful consideration is taken to design the setup such that the combination of inertia and angular velocity provides enough angular momentum to reach the desired position. Such is done through

American Institute of Aeronautics and Astronautics

Table 1. Identified System Parameters

Parameter	Value	Unit
l_b	0.077	m
l_w	0.089	m
m_b	0.436	kg
m_w	0.131	kg
I_b	4.21×10^{-3}	kg m^2
I_w	0.42×10^{-3}	kg m^2
C_b	1.94×10^{-3}	kg m^2 s^{-1}
C_w	0.07×10^{-3}	kg m^2 s^{-1}

Eq. (11) and is also explained in Gajamohan et al.[17]

$$\dot{\varphi}_w = (2\pi \cdot 2) \sqrt{\frac{p - (I_w + I_b + m_w l_w{}^2)}{I_w{}^2}(m_b l_b + m_w l_w)\, g} \tag{11}$$

Figure 2. Jump-up maneuver accomplished by transferring angular momentum from the wheel to the body and pivoting about the hinge point.

Unlike the stopping power of disc brakes via hydraulic pressure in a car, a low-cost RC servo does not possess the torque required to stop the spinning momentum wheel without damaging the servo. Even if it could, the angular momentum transfer would not be instantaneous and would introduce additional system delays and dynamics while degrading the setup's self-erecting ability. Instead, the impulsive force during momentum transfer is carried by the slotted (purple) metal component in Fig. 4, so the servo does not require a high torque rating. The RC servo's task is merely to actuate the (red) metal barrier as quickly as possible. A 0.5-inch 4-40 screw is put into the side of the wheel to create a protrusion on the edge. This creates a contact point for the metal barrier to stop the spinning wheel to achieve momentum transfer.

C.   Material and Component Selection

Since the main goal is to design a low-cost experimental set-up via commercially available, off-the-shelf products, component selection becomes an important part of the design process and is driven by the cost and availability of the material. Selections are made with the 3-D prototype in mind to reduce the overall cost of the project. Components used in the 1-D prototype are directly carried over to the 3-D configuration to reduce development time and production costs.
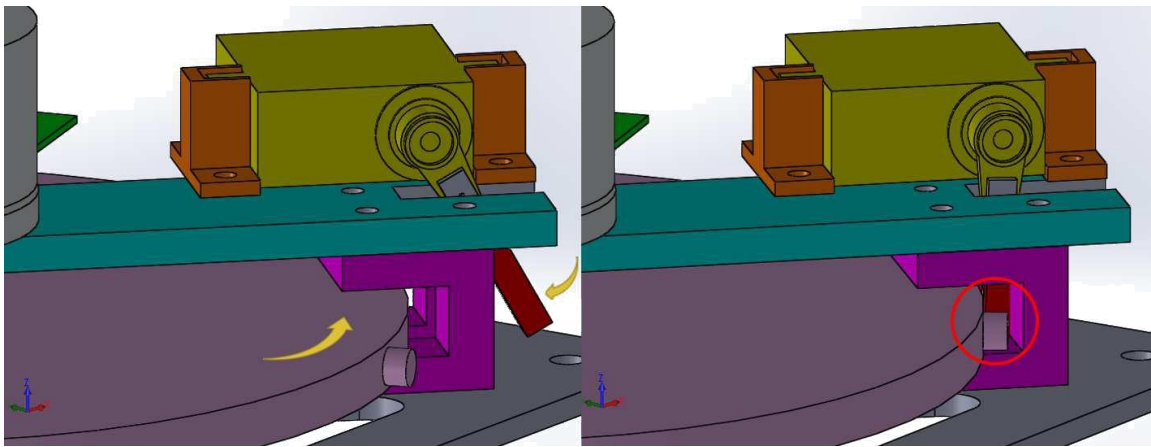
Figure 3. Angular momentum transfer achieved by stopping the momentum wheel via a metal barrier actuated by the RC servo.

Although more expensive than other microcontroller boards, the Arduino Mega 2560 is chosen for the availability of extensive open-source libraries. The MPU-6050 inertial measurement unit (IMU) is used which houses a 3-axis accelerometer and 3-axis gyroscope. Although a single-axis sensor would be su cient for this prototype, a 3-axis solution is chosen with the future 3-D con guration in mind. The HSG-5084MG servo is selected for its unique actuation speed (0.07 sec/60) to minimize associated system delays. The DF45 from Nanotec is implemented for its high torque rating and small form factor. The B12A6 is used since it possesses a current mode that allows for direct control of output torque. Two 12-bit digital-to-analog converters are required to provide an analog voltage output to drive the motor controller since the Arduino Mega does not have an onboard DAC.

Aluminum 6061 is chosen to construct all custom components because of its desirable material properties and cost. It is also easily available in various forms. Custom components are designed using standard dimensions so that purchased material requires minimal machining and fabrication is quick. CNC fabrication can be avoided completely by designing parts that do not require high precision so that the total cost of the project can be further reduced. A complete list of materials and components is given in Table 2.

Table 2. Cost breakdown of the major components.

Component	Manufacturer	Model Number	Price (USD)
Microcontroller	Arduino	Mega 2560	50
Inertial Measurement Unit	InvenSense	MPU-6050	10
65W Brushless DC Motor	Nanotec	DF45	77
Motor Controller	Advanced Motion Controls	B12A6	180
RC Servo	HiTec	HSG-5084MG	30
Raw Material	McMaster Carr	6061 Aluminum Alloy	50
12-bit DACs	Sparkfun	MCP4725	10
		Total*	480

*Total includes miscellaneous items, tax, and shipping costs

D.   Custom Components

The setup calls for ve custom designed components, and those can be seen in Fig. 4. The rst is the (grey) plate (6 x 6 x 0.125 inches) that serves as the main platform and will later serve as a face of the cube on the 3-D prototype. The assembly will pivot about a hole on this plate. The second is a cylindrical (pink) disk (5 inch diameter, 0.25 inch thickness) that serves as the momentum wheel. The third is a (teal) plate (4 x 1 x 0.1875 inches) used to mount the motor/wheel assembly. A fourth (purple) piece holds up the teal plate and provides a slot for the braking mechanism to swing in and contact the stopper at the edge of the wheel.

American Institute of Aeronautics and Astronautics

A fth (red) piece (0.25 x 0.375 x 1.375 inches) will be actuated by the servo and acts as a barrier to stop the spinning momentum wheel.
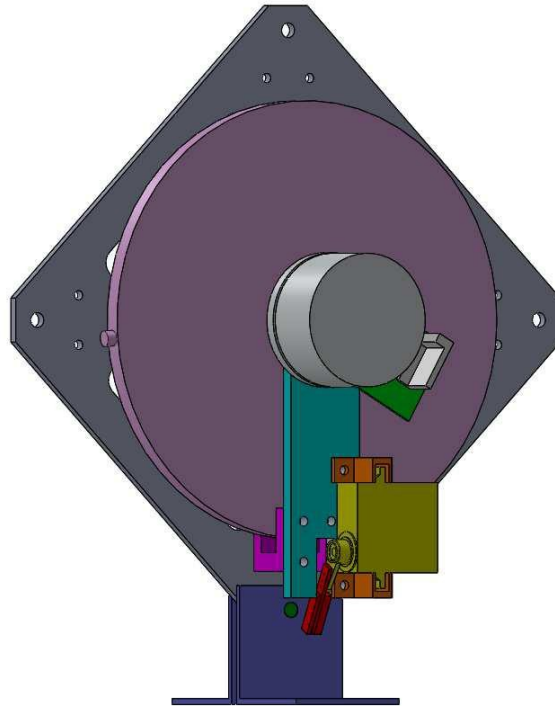

Figure 4. CAD drawings of the 1-D prototype.

E.   Experimental Setup Overview

A basic overview of the experimental setup can be seen in Fig. 5. The accelerometer and gyroscope provide measurements on the tilt angle and tilt rate of the setup, respectively. Hall sensors on the BLDC motor provide a measurement on angular velocity. The Arduino Mega 2560 calculates the current output required through the feedback control law. The current command is mapped to an analog voltage command that can be outputted by the DACs to the motor controller. The motor controller then takes the voltage command and outputs a current command to control the torque output.
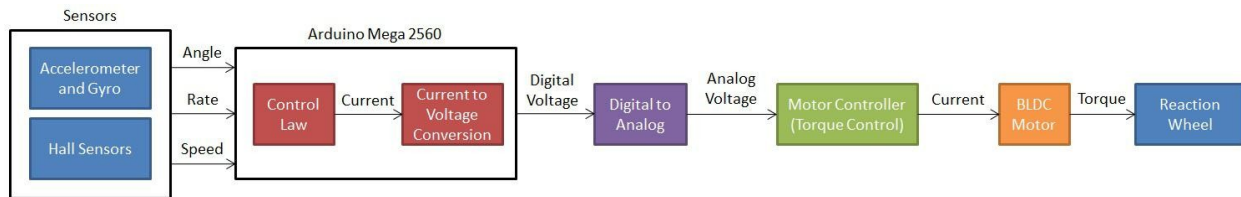

Figure 5. Overview of experimental setup

F.   Complementary Filter Design

It is necessary to calibrate and correct the sensor's measurements for optimal performance. A noisy signal from the raw accelerometer outputs will result in increased energy consumption since the controller will attempt to correct for erroneous angle displacements. Angles obtained from gyroscope measurements will drift over time (3 deg/sec) due to integration, so it is unreliable in the long term. A complementary lter, as shown in Eq. (12), is used to correct for the drift of the gyroscope and lter out the noise from the accelerometer.[21]

American Institute of Aeronautics and Astronautics

$$\theta_b = \alpha(\theta_b + \bar{\omega}_{b;gyro}\,\Delta t) + (1-\alpha)(\theta_{b;accel}) \qquad (12)$$

$$\theta_{b;accel} = \tan^{-1}\left(\frac{g_y}{g_z}\right) - \theta_0 \qquad (13)$$

where $\bar{\omega}_b$ is the angular velocity (deg/sec) output by the gyroscope about an axis. Multiplying the gyroscope output by a time constant (Δt) approximates the integral to provide an angle. $\theta_{b;accel}$ is the angle about an axis computed via the inverse tangent of the accelerometer readings from the other two axes, shown in Eq. (13). α is a weighting factor that determines which signal the complimentary filter follows closer. It is found that $\alpha = 0.98$ provides a relatively clean signal that does not drift over time, as shown in Fig. 6.

Offsets for the gyroscope and accelerometer readings are found by measuring 1000 data points while the sensor is in a static condition (laying down on a flat surface with the z-axis aligned with the local vertical). Measured values are averaged and compared to known values in such an orientation before being used to calibrate the gyroscope and accelerometer. θ_0 is set to 45 deg. to offset the measured angle so that 0 deg. is measured at the balancing reference point.
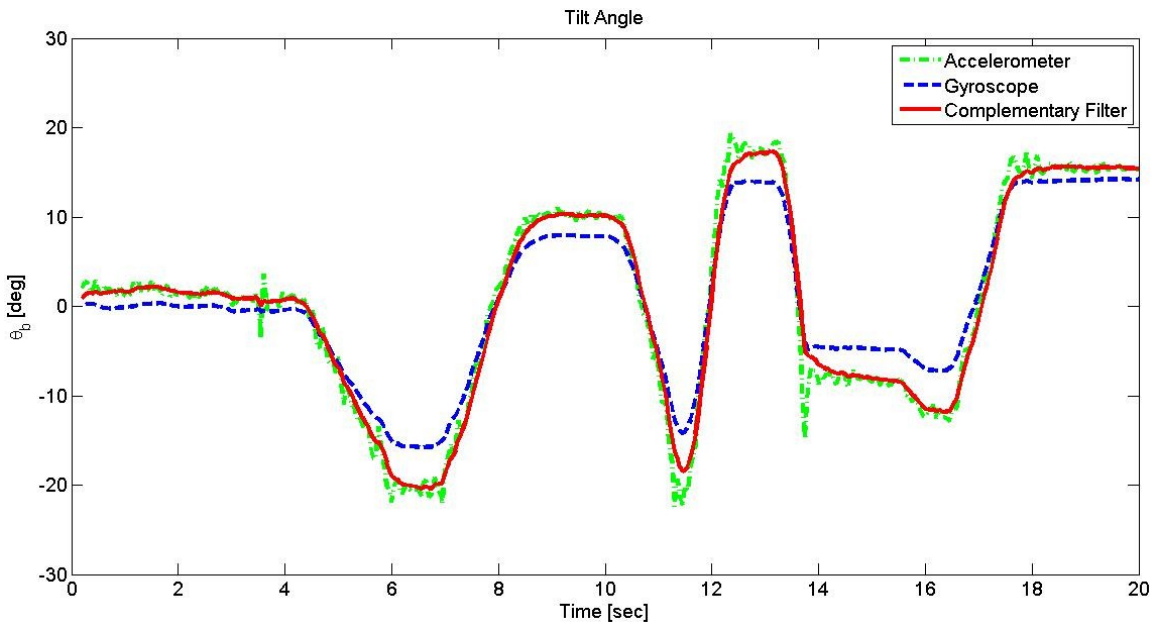

Figure 6. Tilt angle measurements obtained via accelerometer, gyroscope, and complimentary filter.

III. Controller Design

It is important to design controllers with spacecraft performance goals (such as reference tracking or energy consumption minimization) in mind since the setup is to serve as a spacecraft attitude determination and control platform. As such, large emphasis is placed on minimizing controller effort to reduce associated power consumption, thus saving energy and minimize fuel/power consumption. Considering the fact that the life span of satellites is measured with years, even small savings in energy consumption (through reduced control effort) will become substantial over the whole lifetime of a spacecraft. This also has a direct impact on the overall mission objectives and reduces the associated cost of the mission.

To address all those concerns, for this study, two controllers are developed for this purpose. The first is a proportional-integral-derivative (PID) controller.[22]

$$PID(s) = K_p\left(1 + \frac{1}{T_i s} + T_D s\right) \qquad (14)$$

A PID controller is designed to achieve minimal control effort, and will serve as a baseline controller for comparison purposes. A second PID controller is also designed for reference tracking performance. This will provide insight on the performance and reliability of the PID tuner application and process.

A linear quadratic regulator[23] (LQR) is also developed to achieve optimal performance and minimize energy consumption. The LQR controller minimizes the cost function-J via weighting factors, Q and R, that penalize the transient and control energy, respectively, as also shown in Eq. 15.

$$\min J = \int_{t1}^{t2} (x^T Q x + u^T R u)\, dt \tag{15}$$

Two different LQR controllers are also designed for comparison. In the first one, the weighting factors are equally penalizing the transient and control energy, while the second heavily penalizes control energy to minimize the control effort.

IV.   Simulation Results

Preliminary results from both controllers can be seen in Fig. 7 and Fig. 8. The curves in Fig. 8 are numerically integrated to find the total energy consumption of each controller when subjected to the same unitary impulse disturbance. This will be used as a direct measure of the controller's performance. Both the initial and improved LQR controllers provide reductions in energy consumption by 4% and 8% over the baseline PID controller, respectively.
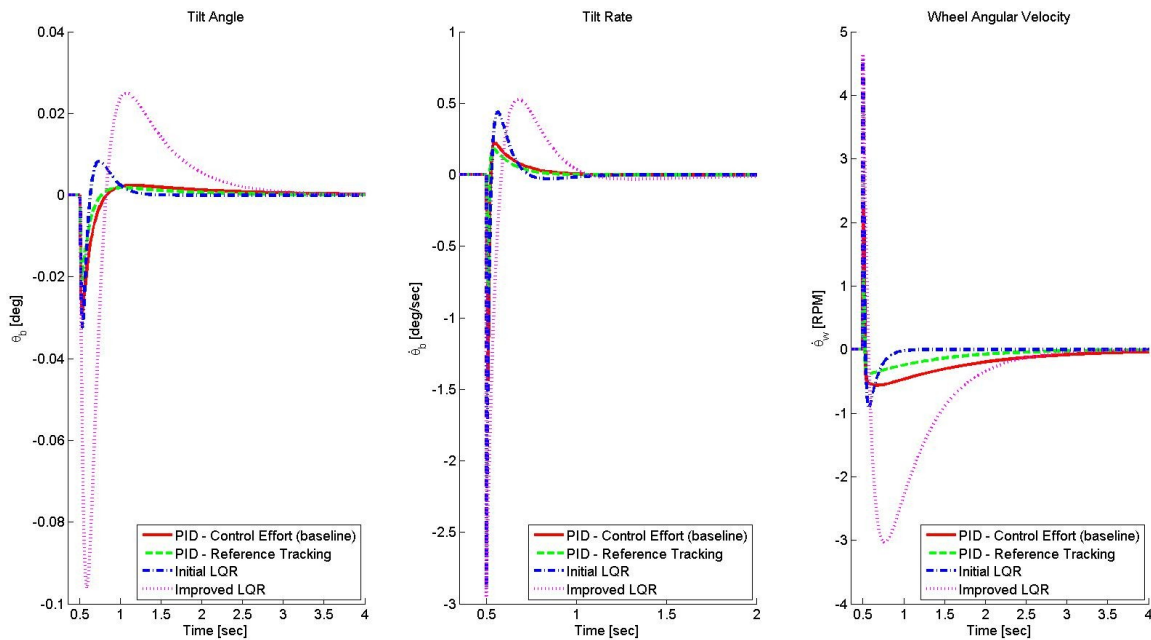

Figure 7. Comparison of PID and LQR controllers for the three states.

The results also indicate PID controllers are difficult to reliably tune for optimal performance since there is no way to ensure that a local minimum has been reached with the current configuration. Various design attempts demonstrated that while the PID can be tuned for best time domain reference tracking performance or minimal control effort, simultaneously optimizing multiple objectives is found to be tedious and time-consuming, therefore impractical. On the other hand, the LQR performed as desired, and will be implemented on the experimental setup as the initial test controller.

Some limitations of the setup are found after the system has been fully identified, where RC servo and DC motor dynamics have yet to be identified, and is excluded from the content of this paper. Results will be included and reported in another future study. The constraints to the maximum tilt angle ($\theta_{b;max}$) will provide bounds for optimal controller design. As long as the maximum tilt angle is not exceeded by a given impulse, the controller can be further improved to lower energy expenditure.

Hardware limitations (such as maximum current or torque) directly influence the setup's dynamics and capabilities. Actuator saturation (primarily the DC motor) is a major constraint that limits the controller's ability to reject disturbances. Such limitations need to be taken into account during controller and model
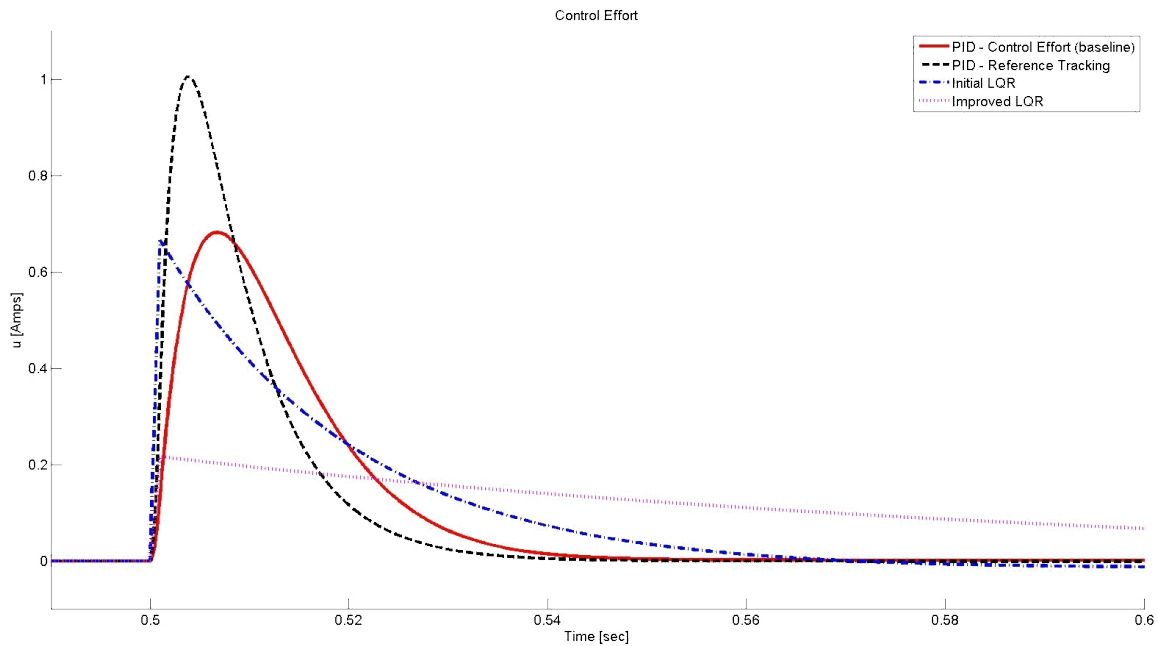
American Institute of Aeronautics and Astronautics

Figure 8. Controller e ort of various PID and LQR controllers.

design. Otherwise, even if the controller demands more performance, the hardware will not be able to follow the commanded inputs, and the desired performance will not be achieved.

V.   Experimental Results

For this portion of the study, the state space is discretized (Eq. 16) and a feedback control law (Eq. 17) is implemented on the Arudino Mega.

$$x[n + 1] = A\,x[n] + B\,u[n]$$
$$y[n] = C\,x[n] + D\,u[n]$$

(16)

$$u[n] = K_{LQR}\,x[n]$$
(17)

However, initial attempts using Simulink's Arduino environment proved unsuccessful. The 25 [Hz] sampling frequency limitation degraded the performance of the LQR controller to the point that the plant could not be stabilized. Fig. 9 characterizes the impact on the controller's performance based on the sampling frequency. In order to improve the performance, Arduino's native IDE is used to program and operate the controller as a standalone unit. The sampling frequency is then able to be increased up to 100 [Hz]. However, to provide extra time for data collection through the serial connection and prevent overrunning, the control loop is run at 50 [Hz].

With the increased sampling frequency, the initial tests of the LQR demonstrated the ability to reject impulse responses. However, as a direct result of an impulse disturbance, the CG of the pendulum shifts and gravity applies a constant torque due to the nonzero tilt angle. The gravity-induced step disturbance generates a nonzero steady state error from the 0-degree (vertical) reference point. This drives the DC motor to produce constant angular acceleration to generate the necessary torque to maintain its new (nonzero) orientation. Once the DC motor reaches the imposed saturation limit, the setup will destabilize.

In order to correct the nonzero steady state error due to gravity, the state space representation is augmented to provide integral action. Namely, the A and B matrices are augmented with a fourth state, the integral of error. The derivative of the fourth state is then simply the error, e, in the tilt angle from the 0-degree reference.

$$e = y\; ref = {}_b$$
(18)

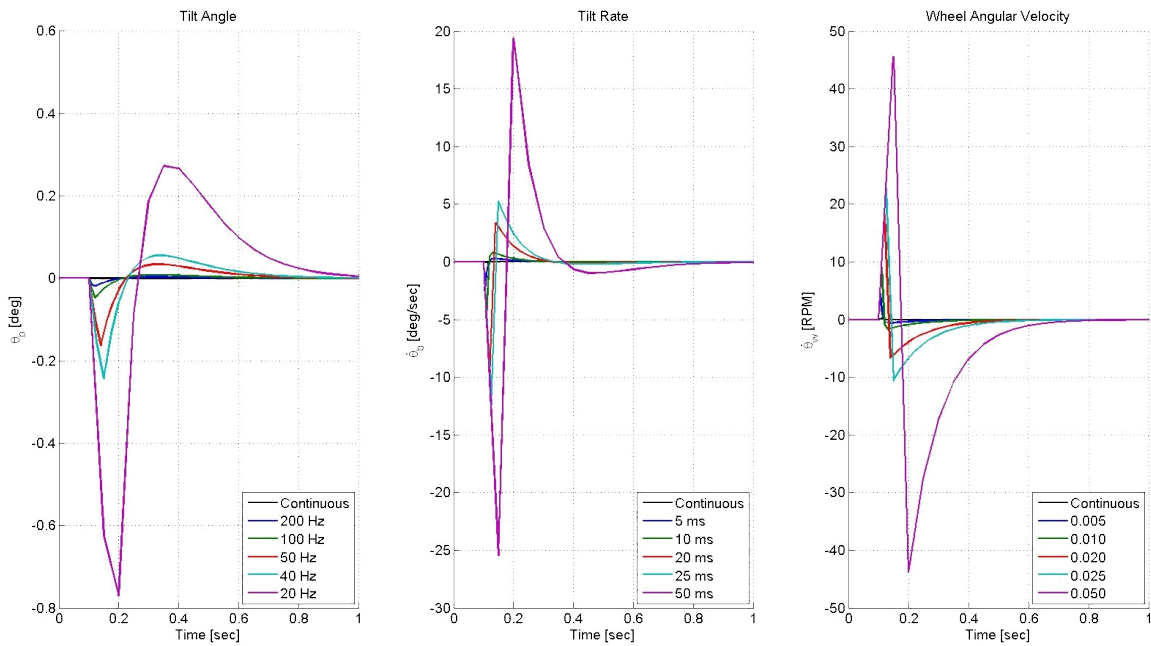American Institute of Aeronautics and Astronautics

Figure 9. Continuous and discrete LQR controller performance for various sampling frequencies.

$$A = \begin{bmatrix} 1 & 0_{1 \times 3} \\ A_{3 \times 3} & 0_{3 \times 1} \end{bmatrix}_{4 \times 4} \qquad B = \begin{bmatrix} 0 \\ B_{3 \times 1} \end{bmatrix}_{4 \times 1} \qquad C = \begin{bmatrix} 1 & 0 & 0 & 0 \end{bmatrix} \qquad (19)$$

$$\begin{bmatrix} \dot{e} \\ \dot{R} \end{bmatrix} = A \begin{bmatrix} e \\ R \end{bmatrix} + B u \qquad (20)$$

A pre lter gain is added to facilitate the elimination of any steady state error. The block diagram of the control strategy can be seen in Fig. 10. Fig. 12 shows that the inclusion of the pre lter gain and integral action is able to eliminate the steady state error in tilt angle and return the pendulum to its vertical reference point, as seen in Fig. 11. Once the pendulum eliminates the error in tilt angle, it begins to eliminiate the error in angular velocity by driving the RPM to zero.
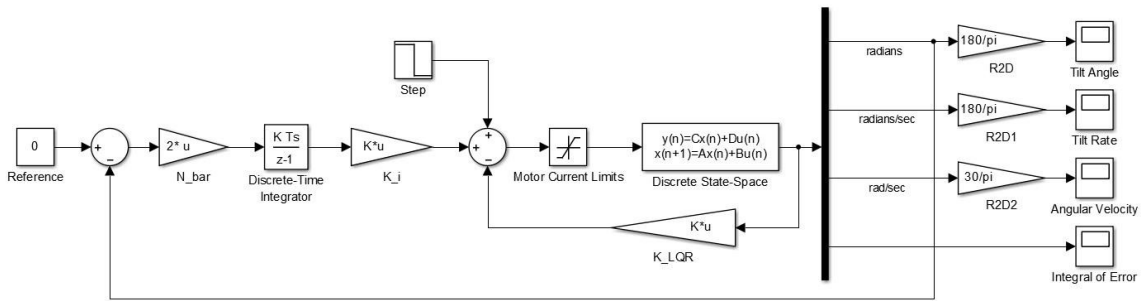

Figure 10. Control strategy including pre lter gain and integral action to eliminate the steady state error in tilt angle.

VI.   Conclusion

In this study, a 1-D prototype has been designed to serve as a spacecraft attitude determination and control research platform. PID and LQR controllers have been designed in Simulink and analyzed for best performance with minimal control e ort. The LQR demonstrated energy savings of up to 8% over the

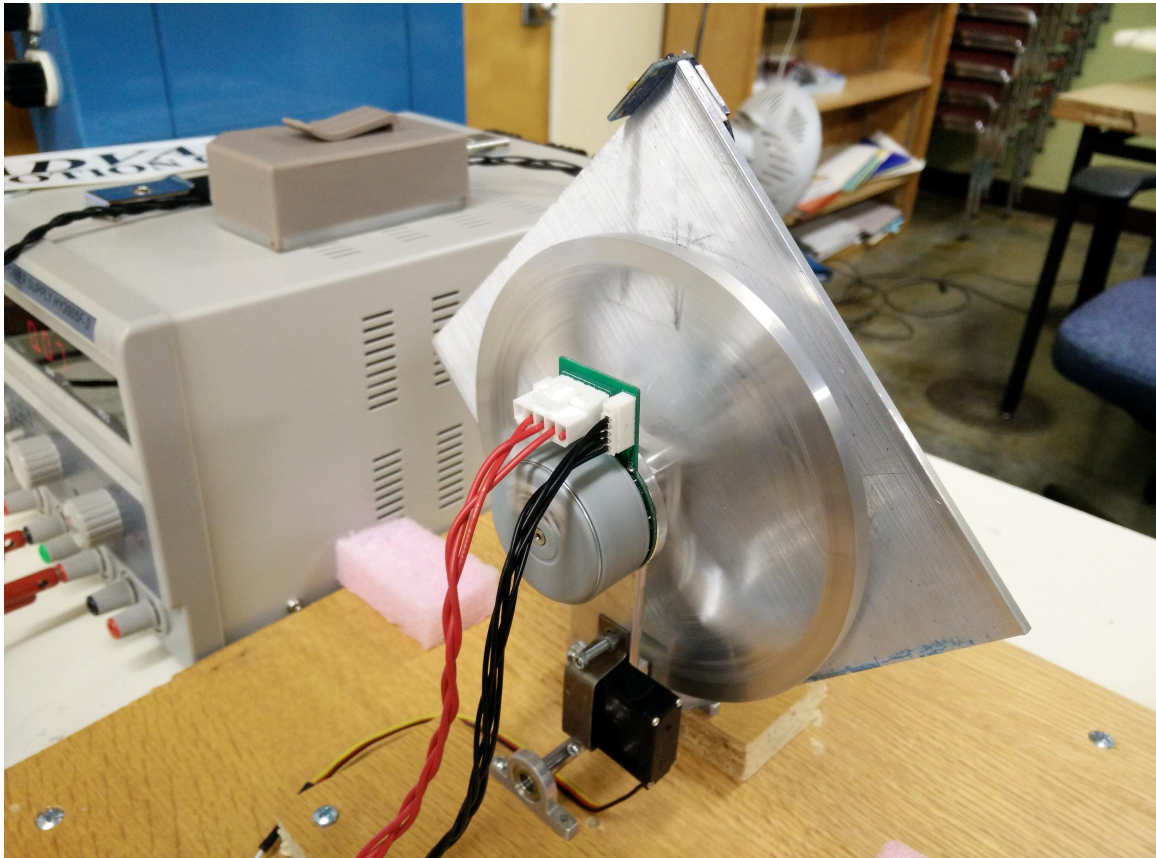American Institute of Aeronautics and Astronautics
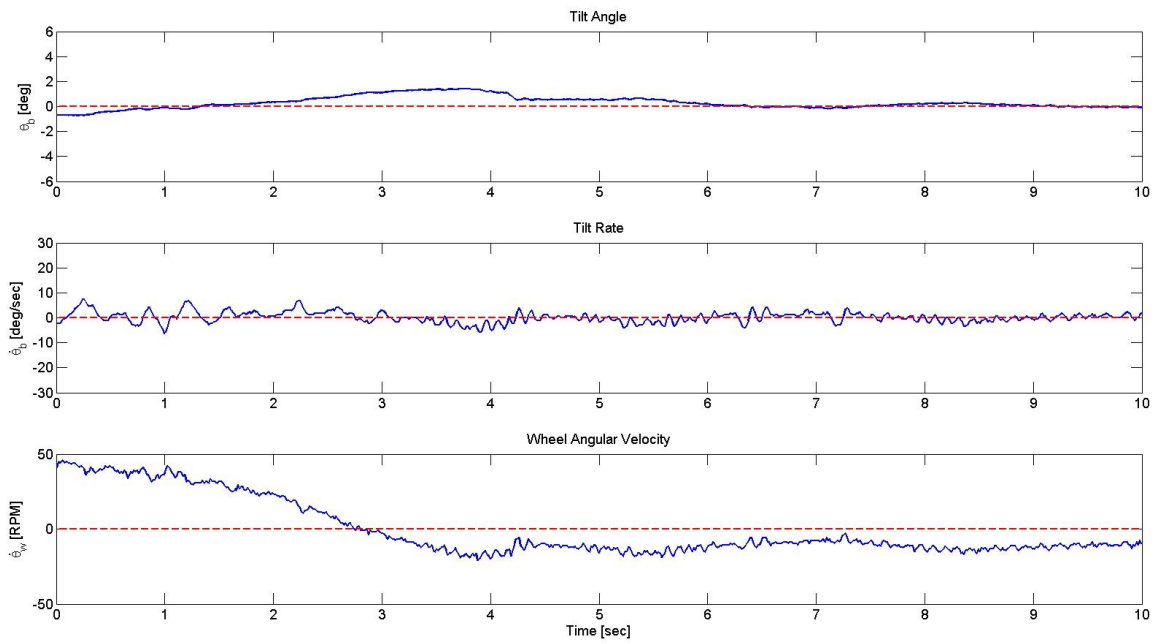
Figure 11. Experimental setup during a balancing maneuver.

Figure 12. Time history of the tilt angle, tilt rate, and angular velocity for a 10 second balancing experiment.

American Institute of Aeronautics and Astronautics

PID in simulation. Initial attempts to streamline the controller design process through Simulink's Arduino environment was unsuccessful due to sampling time limitations. The Arduino Mega is used as a standalone controller to overcome the issue. As a result, future designs will need to be programmed conventionally without the luxury of a graphical interface that can directly autocode controllers. A LQR was implemented on the experimental setup, but it was not able to reject the step disturbance due to gravity following an impulse. A pre lter gain and integral action is added to the augmented state space representation, and the setup is able to reject both impulses and step disturbances and balance successfully. Total (including tax and shipping) cost was kept to a minimum ($480).

System identi cation will be performed to obtain a more accurate open-loop state-space representation. Various controllers will be tested on the 1-D prototype and experimental results on their energy consumption will be collected for analysis. A more durable braking mechanism is currently under development for the jump-up maneuver. Once complete, the 3-D setup will be manufactured by reproducing the 1-D version and assembling the 3-axis controlled spacecraft.

VII.   Acknowledgments

References

[1] Fleeter, R. and Warner, R., \Guidance and Control of Miniature Satellites," Automatic Control in Aerospace 1989 , IFAC Symposia Series, Pergamon, Oxford, 1990, pp. 243 { 248.

[2] Devey, W. J., Field, C. F., and Flook, L., \An Active Nutation Control System for Spin Stabilised Satellites," Automatica, Vol. 13, No. 2, March 1977, pp. 161{172.

[3] Azor, R., \Momentum Management and Torque Distribution in a Satellite with Reaction Wheels," Israel Society of Aeronautics and Astronautics, 33rd Israel Annual Conference on Aviation and Astronautics, Feb. 1993, pp. 339{347.

[4] Brown, C., Elements of Spacecraft Design, AIAA education series, American Institute of Aeronautics & Astronautics, 2002.

[5] Iwens, R., Fleming, A., and Spector, V., \Precision Attitude Control with a Single Body-Fixed Momentum Wheel," Mechanics and Control of Flight Conference, Feb. 1993, pp. 339{347.

[6] Jung, D. and Tsiotras, P., \A 3-DoF Experimental Test-Bed for Integrated Attitude Dynamics and Control Research," AIAA Guidance, Navigation and Control Conference, Austin, TX , John Wiley & Sons, 2003, pp. 03{5331.

[7] Peck, M. A. and Cavender, A. R., \An Airbearing-Based Testbed for Momentum-Control Systems and Spacecraft Line of Sight," Proceedings of the 13th AAS/AIAA Space Flight Mechanics Winter Meeting, no. AAS 03-127, 2003, pp. 427{446.

[8] Schwartz, J. L., Peck, M. A., and Hall, C. D., \Historical Review of Air-Bearing Spacecraft Simulators," Journal of Guidance, Control and Dynamics, Vol. 26, No. 4, 2003, pp. 513{522.

[9] Crowell, C. W., Development and Analysis of a Small Satellite Attitude Determination and Control System Testbed, Ph.D. thesis, Massachusetts Institute of Technology, 2011.

[10] Kim, B. M., Velenis, E., Kriengsiri, P., and Tsiotras, P., \Designing a Low-Cost Spacecraft Simulator," Control Systems, IEEE, Vol. 23, No. 4, Aug 2003, pp. 26{37.

[11] Iwakura, A., Tsuda, S.-i., and Tsuda, Y., \Feasibility Study on Three Dimensional Reaction Wheel," Proceedings of the School of Science of Tokai University, Series E 33 , 2008, pp. 51{57.

[12] Gui, H., Jin, L., and Xu, S., \Attitude Maneuver Control of a Two-Wheeled Spacecraft with Bounded Wheel Speeds," Acta Astronautica, Vol. 88, No. 0, 2013, pp. 98 { 107.

[13] Bayadi, R., Banavar, R. N., and Chang, D. E., \Characterizing the Reachable Set for a Spacecraft with Two Rotors," Systems & Control Letters, Vol. 62, No. 6, 2013, pp. 453 { 460.

[14] Xinsheng, G., Qizhi, Z., and Li-Qun, C., \Optimal Motion Planning for a Rigid Spacecraft with Two Momentum Wheels using Quasi-Newton Method," Acta Mechanica Solida Sinica, Vol. 19, No. 4, 2006, pp. 334 { 340.

[15] Ismail, Z. and Varatharajoo, R., \A Study of Reaction Wheel Con gurations for a 3-Axis Satellite Attitude Control," Advances in Space Research, Vol. 45, No. 6, 2010, pp. 750 { 759.

[16] Spong, M. W., Corke, P., and Lozano, R., \Nonlinear Control of the Reaction Wheel Pendulum," Automatica, Vol. 37, No. 11, 2001, pp. 1845 { 1851.

[17] Gajamohan, M., Merz, M., Thommen, I., and D'Andrea, R., \The Cubli: A Cube that can Jump Up and Balance," International Conference on Intelligent Robots and Systems, 2012, pp. 3722{3727.

[18] Meyer, J., Delson, N., and de Callafon, R. A., \Design, Modeling and Stabilization of a Moment Exchange Based Inverted Pendulum," 15th IFAC Symposium on System Identi cation, 2009, pp. 462{467.

[19] Sidi, M., Spacecraft Dynamics and Control: A Practical Engineering Approach, Cambridge Aerospace Series, Cambridge University Press, 1997.

[20] \Solidworks 2014, available at http://www.solidworks.com," .

[21] Coopmans, C., Jensen, A., and Chen, Y., \Fractional-Order Complementary Filters for Small Unmanned Aerial System Navigation," Journal of Intelligent & Robotic Systems, Vol. 73, No. 1-4, 2014, pp. 429{453.

[22] Franklin, G., Powell, J., and Emami-Naeini, A., Feedback Control of Dynamic Systems, No. v. 10 in Alternative Etext Formats, Pearson, 2010.

[23] Ogata, K., Modern Control Engineering, Instrumentation and Controls Series, Prentice Hall, 2010.

[24] Muehlebach, M., Mohanarajah, G., and D'Andrea, R., \Nonlinear Analysis and Control of a Reaction Wheel-based 3D Inverted Pendulum," proc. Conference on Decision and Control, 2013, pp. 1283{1289.

[25] Gajamohan, M., Muehlebach, M., Widmer, T., and D'Andrea, R., \The Cubli: A Reaction Wheel Based 3D Inverted Pendulum," proc. European Control Conference, 2013, pp. 268{274.

American Institute of Aeronautics and Astronautics